The FEBS Journal, Volume 282, Issue 20, October 2015, pp3986–4000
DOI: 10.1111/febs.13400

Biochemical Characterisation & Selective Inhibition of β-Carotene *cis-trans*-Isomerase D27 and Carotenoid Cleavage Dioxygenase CCD8 on the Strigolactone Biosynthetic Pathway

Peter J. Harrison[1], Sophie A. Newgas[1], Flora Descombes[1], Sarah A. Shepherd[1], Andrew J. Thompson[2], and Timothy D. H. Bugg[1*]

[1]Department of Chemistry, University of Warwick, Coventry CV4 7AL, UK

[2]Cranfield Soil and Agrifood Institute, Cranfield University, Cranfield MK43 0AL, UK

*To whom correspondence should be addressed: Prof. Timothy D. H. Bugg, Department of Chemistry, University of Warwick, Coventry CV4 7AL, UK. Tel: 44-02476-573018; Fax: 44-02476-524112; Email: T.D.Bugg@warwick.ac.uk

Running title: Inhibition of isomerase D27 and dioxygenase CCD8

Keywords: Strigolactone biosynthesis, carotenoid cleavage dioxygenase, CCD7, CCD8, D27, enzyme inhibition, hydroxamic acid.

ABSTRACT

The first three enzymatic steps of the strigolactone biosynthetic pathway catalysed by β-carotene *cis-trans* isomerase Dwarf27 (D27) from *Oryza sativa* and carotenoid cleavage dioxygenases CCD7 and CCD8 from *Arabidopsis thaliana* have been reconstituted *in vitro*, and kinetic assays have been developed for each enzyme, in order to develop selective enzyme inhibitors. Recombinant OsD27 shows a UV-vis λ_{max} at 422 nm, and is inactivated by silver (I) acetate, consistent with the presence of an iron-sulfur cluster that is used in catalysis. OsD27 and AtCCD7 are not inhibited by hydroxamic acids that cause shoot branching *in planta*, but OsD27 is partially inhibited by terpene-like hydroxamic acids. The reaction catalysed by AtCCD8 is shown to be a two-step kinetic mechanism using pre-steady state kinetic analysis. Kinetic evidence is presented for acid-base catalysis in the CCD8 catalytic cycle, and the existence of an essential cysteine residue in the CCD8 active site. AtCCD8 is inhibited in a time-dependent fashion by hydroxamic acids D2, D4, D5 and D6 (>95% inhibition @ 100 μM) that cause a shoot branching phenotype in *Arabidopsis thaliana*, and selective inhibition of CCD8 is observed using hydroxamic acids D13H and D15 (82%, 71% inhibition @ 10 μM). The enzyme inhibition data implies that the biochemical basis of the shoot branching phenotype is due to inhibition of CCD8.

INTRODUCTION

Carotenoids, long chain C_{40} polyene terpenoids produced by phototrophic organisms, are broken down to apocarotenoids by a family of enzymes known as the carotenoid cleavage dioxygenases (CCDs) [1,2]. CCDs are non-heme iron-dependent enzymes that catalyse the oxidative cleavage of the polyene backbone of a carotenoid or apocarotenoid substrate. Vp14 (NCED1) from *Zea mays* was the first biochemically characterised CCD enzyme [3], and is responsible for the 11,12 cleavage of 9'-*cis*-neoxanthin and/or 9'-*cis*-violaxanthin in the biosynthesis of the plant hormone abscisic acid (ABA), an inhibitor of seed germination, and mediator of plant responses to drought [4-6].

Since the discovery of Vp14, CCDs have been identified across all taxa and have been shown to be involved in the biosynthesis of a range of apocarotenoids. In mammals, the enzyme *β*-carotene oxygenase I is required for the biosynthesis of visual pigment 11-*cis*-retinal [7,8]. In plants, strigolactones have been identified as hormones involved in rhizosphere signalling, and as inhibitors of shoot branching [9-11]. Biosynthesis of strigolactones requires the action of two CCD enzymes, CCD7 and CCD8, which act sequentially on 9-*cis*-*β*-carotene, as shown in Figure 1 [12]. The biosynthetic pathway begins with the isomerisation of all-*trans*-*β*-carotene to 9-*cis*-*β*-carotene catalysed by Dwarf27 (D27) [12,13]. Oxidative cleavage of 9-*cis*-*β*-carotene at the 9′,10′ position is then catalysed by CCD7, to produce 9-*cis*-*β*-apo-10'-carotenal [12]. CCD8 catalyses an unusual double oxygenation of 9-*cis*-*β*-apo-10′-carotenal to produce an intermediate known as carlactone [12]. Carlactone is then oxidised by consecutive P450 enzyme oxidations to give *ent*-2′-*epi*-5-deoxystrigol: recombinant *Arabidopsis* Max1 has been shown to form carlactonoic acid [14], whereas a recombinant Max1 homolog from *Oryza sativa* (called carlactone oxidase) has been shown to form *ent*-2′-*epi*-5-deoxystrigol directly [15].

Figure 1. Strigolactone biosynthetic pathway

A number of CCD enzymes have been structurally characterised, revealing a conserved seven bladed β-propeller motif within the protein structure [16, 17]. The catalytic iron (II) centre is co-ordinated by four histidine residues, an unusual ligand set for non-heme-iron dependent dioxygenase enzymes [2, 18].

In view of the physiological effects of abscisic acid and strigolactones, there is interest in the development of selective inhibitors for the carotenoid cleavage dioxygenases [2]. The first compounds shown to inhibit CCDs were the tertiary amine compounds abamine and abamineSG, which inhibit NCED on the abscisic acid biosynthesis pathway [19, 20]. AbamineSG was shown to inhibit *Vigna unguiculata* NCED1 with a K_i of 18.5 μM [20]. *In planta*, both abamine and abamineSG inhibited ABA biosynthesis [19,20]. Inhibition of *Arabidopsis thaliana* NCED3 has been reported by sesquiterpene-like compounds, the most effective compound showing K_i 93 μM [21].

A collection of substituted hydroxamic acid compounds have been shown to inhibit CCD enzymes NCED1 and CCD1 from *Solanum lycopersicum* [22]. Against NCED1, the most effective compound, D8, showed 40% inhibition at 100 μM, whilst against CCD1, IC_{50} values of <1 μM were reported [22]. *In planta* phenotypic effects have been observed in *Arabidopsis* with a number of different hydroxamic acid inhibitors. Compounds D4 and D6 were shown to cause an increase in the number of shoot branches, suggesting inhibition of a CCD enzyme involved in SL biosynthesis [22]. Additionally, smaller hydroxamic acids F1 and F2 have been shown to cause a bleaching phenotype, due partly to inhibition of the enzyme *p*-hydroxyphenylpyruvate dioxygenase, but also a second unknown metalloenzyme target [23]. A phenotypic effect on lateral root branching has been observed with the compound D15, believed to result from the inhibition of the biosynthesis of an unknown apocarotenoid signalling molecule [24].

To date, no selective inhibitors of the CCD enzymes CCD7 and CCD8 have been reported. Here we report further biochemical characterisation of the first three enzymes on the strigolactone biosynthesis pathway, screening of these enzymes against previously reported and new hydroxamic acid based compounds, and the identification of inhibitors for D27 and CCD8.

RESULTS

Preparation of novel hydroxamic acids. In addition to the collection of hydroxamic acids described previously [22-24], 8 novel hydroxamic acids were synthesised, using a modification of the synthetic route previously described [22]. In order to mimic the terpenoid backbone of the strigolactone biosynthetic pathway intermediates, three terpene-like hydroxamic acids were prepared: compound D30 contains an *N*-

substituted C_{10} geranyl unit; while compounds D31 and D32 contain *C*-substituted C_{10} and C_{12} terpenoid units respectively. Since CCD8 catalyses oxidative cleavages more distant from the carbocyclic ring of its substrate *β*-apo-10'-carotenal, hydroxamic acid B2 containing a 5-atom spacer between the oxygenated aromatic ring and the hydroxamic acid functional group, and compounds D12H and D13H containing a 2-carbon spacer were available from another study of metallo-oxygenase inhibition [25]. Finally, two compounds D20 and D21 containing a more water-soluble carboxylic sidechain were also prepared. The chemical structures are shown in Table 1.

Biochemical Characterisation of OsD27. OsD27 was expressed in *E. coli* as a glutathione-S-transferase fusion protein, and purified using affinity chromatography. The D27-catalysed reaction was monitored *in vitro* using C_{30} reverse phase HPLC, observing the change in ratio between the all-*trans* (retention time 23.9 min) and 9-*cis* (retention time 24.5 min) isomers of *β*-carotene. Isomers of *β*-carotene were identified by their UV-Vis spectra with reference to published values [12, 26, 27]. Commercially available *β*-carotene was found to contain approximately 2% 9-*cis*-*β*-carotene (see Figure 2C). Addition of recombinant D27 to the commercially available *β*-carotene resulted in little change in the ratio of the two isomers (see Figure 2D). In order to test the D27 reaction *in vivo*, the pGEX-OsD27 expression vector was transformed into genetically engineered *E. coli* strain pAC-BETA, which accumulates *β*-carotene [28], and the carotenoid products extracted for HPLC analysis. As shown in Figure 2B, introduction of the expression vector containing OsD27 leads to an increase of 31% in the amount of 9-*cis*-*β*-carotene, compared to pAC-BETA alone.

Figure 2. OsD27 HPLC Assay.

The reverse reaction catalysed by OsD27 was then examined by HPLC purification of 9-*cis*-*β*-carotene (see Figure 2E), followed by addition of recombinant OsD27, which resulted in the formation of 2:1 all-*trans*-*β*-carotene:9-*cis*-*β*-carotene, with a calculated equilibrium constant of 0.53 between the isomers (see Figure 2F). A smaller additional peak at retention time 21.6 min was observed in the HPLC trace for the

D27-catalysed reaction (see Figure 2F), indicating that D27 can generate a second reaction product in the reverse reaction, with λ_{max} 443 nm. Incubation of purified 9-*cis*-*β*-carotene under the enzyme assay conditions gave rise to no measurable increase in all-*trans*-*β*-carotene, indicating that the background rate of non-enzymatic isomerisation is low. The K_M for 9-*cis*-*β*-carotene in the reverse reaction was determined to be 0.26 μM, with a k_{cat} value of 34 s^{-1}.

OsD27 has been previously reported to contain iron [15], but the precise nature of the iron cofactor is uncertain. The purified recombinant OsD27 from our protocol was found to show a UV-vis absorbance maximum at 422 nm (see Figure 3), in agreement with that observed by Lin *et al*. [15], and consistent with λ_{max} values observed for proteins containing [2Fe2S] clusters [29,30]. In order to probe the identity of this species, recombinant OsD27 was treated with mild oxidising and reducing agents. In contrast to the observations of Lin *et al*., no change in the absorbance spectra was observed on addition of 100 μM sodium dithionite, and no loss of catalytic activity was observed upon addition of either 100 μM sodium dithionite or 100 μM hydrogen peroxide. However, a decrease in intensity of the peak at 422 nm was observed on addition of 100 μM silver (I) acetate (see Figure 3), a reagent that is reported to inactivate proteins containing [4Fe4S] clusters [31]. Addition of silver acetate was also found to completely inhibit the isomerisation of 9-*cis*-*β*-carotene by OsD27 via HPLC assay (see Figure 4B).

Figure 3. UV-Vis spectrum of recombinant OsD27

Figure 4. Kinetic analysis of OsD27

In order to probe further the mechanism of isomerisation catalysed by OsD27, a pH-rate profile of OsD27 was determined, which showed <2-fold variation in the rate of isomerisation of 9-*cis* to all-*trans*-*β*-carotene over pH range 4-10 (see Figure 4A), hence there is no apparent acid-base catalysis. Additionally, the reaction was carried out anaerobically under an atmosphere of nitrogen, which resulted in the same ratio of 9-*trans*:9-*cis* products, (see Figure 4B), indicating that OsD27 does not require dioxygen for activity.

Inhibition of OsD27 by hydroxamic inhibitors. Hydroxamic acid inhibitors were tested against OsD27 at a final concentration of 100 μM (see Table 1) by monitoring the isomerisation of 9-*cis*-*β*-carotene to all-*trans*-*β*-carotene. At 100 μM only partial inhibition was observed: most inhibition was observed by the terpene-like compounds D30, D31, and D32 (41%, 38% and 33% inhibition respectively), and by compounds B2 (40% inhibition) and D12H (40% inhibition). Compounds D2, D4, D5 and D6 that show a shoot branching phenotype *in planta* [22] gave no inhibition at all, while low levels of inhibition were observed with the shorter compounds F1-6.

Table 1. Inhibition of OsD27 and AtCCD8 by hydroxamic acids

Biochemical characterisation of AtCCD7. AtCCD7 was expressed with a GST fusion tag, and showed improved expression in *E. coli* containing plasmid pBB541 expressing GroES/EL. Recombinant AtCCD7 was purified by GST affinity chromatography. The CCD7 cleavage reaction was monitored *in vitro* using C_{30} reverse HPLC (see Figure 5). The presence of product *β*-apo-10′-carotenal was confirmed by HRMS and was assigned as the 9-*cis* isomer by comparison of the λ_{max} (444 nm) to published values [9]. A K_M value of 8.7 μM was determined for CCD7 using the HPLC-purified 9-*cis*-*β*-carotene substrate.

Figure 5. HPLC assay of AtCCD7.

Hydroxamic acid compounds and abamine were tested as inhibitors of AtCCD7 at a final concentration of 100 μM. Surprisingly, none of the compounds tested were found to show any inhibition of the AtCCD7-catalysed reaction, nor was any inhibition observed after pre-incubation with enzyme. Hence AtCCD7 is much less susceptible to inhibition by hydroxamic acids than other CCD enzymes studied [22].

Biochemical Characterisation of AtCCD8. AtCCD8 lacking the first 168 base pairs (corresponding to a chloroplast transit peptide) was expressed with an N-His_6 affinity tag and purified by N-His_6 affinity chromatography. Substrate *β*-apo-10'-carotenal was generated by the preceding enzyme CCD7. Monitoring of the CCD8 reaction by C_{30} reverse phase HPLC analysis showed the disappearance of substrate *β*-apo-10′-

carotenal, and monitoring by UV-VIS spectroscopy was found to give a time-dependent decrease in absorbance at 430 nm, which was dependent upon the concentration of enzyme added, with no change observed using deactivated enzyme (see Figure 6A,B). A new product peak was observed via HPLC analysis on a C_{18} reverse phase column at retention time 15.2 min, which showed λ_{max} 267 nm, matching the data of Alder et al for the product carlactone [12]. Attempts to characterise this peak by electrospray mass spectrometry were unsuccessful, suggesting that the product is chemically unstable. Although Alder et al obtained mass spectral data for carlactone, the enol ether functional group present in carlactone is susceptible to hydrolysis in aqueous solution [32]. Treatment of the CCD8 organic extract with alkaline sodium borohydride gave new species at *m/z* 209.2 and 143.1 by electrospray mass spectrometry, consistent with the expected structures of the reduced C_{14} portion of carlactone, and the reduced C_8 by-product of the CCD8 reaction, respectively, as shown in Figure 6C. Our data are therefore consistent with the CCD8-dependent conversion of *β*-apo-10′-carotenal to carlactone [12], which in our hands was chemically unstable.

Figure 6. Continuous UV-vis assay for AtCCD8

Kinetic experiments revealed that substrate inhibition was observed at >15 μM substrate concentration. Kinetic data was modelled using the analysis software GraphPad, and a K_M value of 9.2 μM and specific activity of 2.48 $x10^{-1}$ μmol mg^{-1} s^{-1} was determined for the 9-*cis*-*β*-apo-10′-carotenal substrate, giving an estimated k_{cat} value of 0.18 s^{-1}. The pre-steady state kinetic behaviour of AtCCD8 was investigated using UV-vis stopped-flow kinetic analysis. Upon mixing of a 1:1 molar ratio of AtCCD8 to substrate 9-*cis*-*β*-apo-10′-carotenal, a decrease in absorbance at 440 nm was observed over 40 s (see Figure 7). Analysis of the data showed that the decay at 440 nm could be fitted accurately by a biphasic exponential function, with kinetic parameters A=0.139, k_1=0.43 s^{-1} and k_2=0.06 s^{-1}. While it is of some concern that k_2 is slower than the estimated k_{cat} value, calculation of k_{cat} involves the protein concentration estimated by Bradford assay using bovine serum albumen as standard, which could over- or under-estimate the true protein concentration, and also involves the extinction coefficient for 9-*cis*-*β*-apo-10′-carotenal, which may vary in magnitude between different buffers and pH.

Figure 7. Stopped-flow kinetic data for AtCCD8

A pH rate profile of CCD8-catalysed consumption of 9-*cis*-*β*-apo-10′-carotenal shows inflexions at pH 6.0 and pH 8.0 (see Figure 8), indicating the presence of a catalytic base of pK_a 6.0, and a catalytic acid of pK_a 8.0. The identity of active site groups was probed via incubation of AtCCD8 with a range of group specific reagents at 1 mM concentration. Complete loss of activity was observed upon treatment of AtCCD8 with cysteine-directed reagents *N*-ethyl maleimide or iodoacetamide, consistent with the presence of an active site cysteine residue [33,34]. Loss of activity was also observed using 1-ethyl-3-(3-dimethylaminopropyl) carbodiimide (EDC), or using diethyl pyrocarbonate, but no inhibition was observed using succinic anhydride (see Figure 8).

Figure 8. pH rate profile for AtCCD8

Inhibition of AtCCD8 by hydroxamic acids. AtCCD8 was screened against the collection of hydroxamic inhibitors initially at a concentration of 100 μM, and then at 10 μM for the most effective inhibitors (see Table 1). Inhibition of the CCD8 cleavage reaction was seen by many hydroxamic acids in the D and F series at 100 μM concentration. Inhibition was found to be strongly time-dependent, giving only a small amount of inhibition with no pre-incubation, but >95% inhibition after 10 min pre-incubation. Inhibition was also observed using abamine, but no inhibition was observed using the larger abamineSG. Inhibition of AtCCD8 was only observed by a smaller group of compounds at 10 μM concentration. Most effective inhibition was observed by compounds D13H (82%), D15 (71%), D12 (56%) and D9 (54%) containing a 2-carbon unit between the aryl group and the hydroxamic acid functional group. Inhibition was observed by compounds D6 (53%), D4 (17%) and D5 (9%) containing a 1-carbon spacer that show a shoot branching phenotype *in planta* [22], but less inhibition was observed by compound D2, and by the shorter F series in which the hydroxamic acid is linked directly to the hydroxamic acid. Compounds with aryl-N lengths above three (such as compounds B1, B2, D30, D31 and D32), were not active at 10 μM concentration.

DISCUSSION

Biochemical characterisation of OsD27. Dwarf27 was first identified by Lin *et al.* in 2009 as an iron-containing enzyme of unknown function [13], but was later identified as an isomerase enzyme responsible for the isomerisation of all-*trans*-*β*-carotene to 9-*cis*-*β*-carotene [12]. Our studies have confirmed this isomerase activity, which gives only a small change in the ratio of all-*trans*:9-*cis* isomers from all-*trans*-*β*-carotene, but a much greater change is evident when assayed in the reverse direction, using 9-*cis*-*β*-carotene as substrate. Interestingly, a small amount of a second product is formed using 9-*cis*-*β*-carotene as substrate, which may perhaps be the 9-*cis*,9′-*cis* isomer, or another isomer of *β*-carotene. The K_M for 9-*cis*-*β*-carotene was found to be 0.26 μM, implying that D27 binds the 9-*cis* isomer with a high affinity, which may lead to product inhibition in the forward direction, and hence the low conversion in the *trans* to *cis* direction.

The UV-vis spectrum of purified OsD27 was found to contain an absorbance peak at λ_{max} 422 nm, agreeing with the value reported by Lin *et al*. [13], similar to λ_{max} values shown by proteins containing [2Fe2S] iron-sulfur clusters. This absorbance peak was removed by addition of silver (I) acetate, which is known to cause the breakdown of iron-sulfur clusters [31]. Catalytic activity was also lost by treatment with silver (I) acetate, implying that this cofactor is required for catalysis, though the resistance to treatment with oxidising and reducing agents implies that it is not readily accessible by solvent. These two observations suggest that OsD27 contains a [2Fe2S] iron-sulfur cluster that is required for catalysis.

In order to probe the mechanism of isomerisation catalysed by OsD27, a pH-rate profile was carried out, but <2 fold variation in the rate of the reaction was observed over pH range 4-10. If the mechanism of isomerisation involved protonation of the polyene chain to form a carbocation, followed by deprotonation, then one would expect to see evidence of acid-base catalysis in the pH-rate profile, which was not observed. Furthermore, it was found that OsD27 retains catalytic activity under anaerobic conditions, therefore it does not require dioxygen for activity. Hence we propose a catalytic mechanism for OsD27 involving a 1-electron transfer from the polyene π-system of *β*-carotene to a [2Fe2S] cluster, generating a radical cation, which is able to rotate about the C-C single bond. Electron transfer back from the reduced [2Fe2S] cluster would then

generate the 9-*cis*-*β*-carotene product. A mechanism involving single electron transfer from a [2Fe2S] cluster to form a radical anion intermediate is also possible.

Figure 9 – Proposed catalytic mechanism for OsD27

OsD27 is not strongly inhibited by the collection of hydroxamic acid metallo-oxygenase inhibitors, as would be expected if there is no mononuclear iron centre, however, up to 40% enzyme inhibition was observed, notably by the terpene-like hydroxamic acids whose structure most closely resembles that of the substrates for OsD27.

Biochemical characterisation of AtCCD7. CCD7 was first identified by Schwartz *et al.* in 2004, and was initially believed to act on all-*trans*-*β*-carotene, performing a 9,10 cleavage reaction to generate *β*-apo-10-carotenal [34,35]. However, the identification of OsD27 as a *β*-carotene isomerase by Alder *et al* led them to propose that CCD7 in fact cleaves the 9-*cis* isomer of *β*-carotene [12]. Our assays of AtCCD7 in the presence of 9-*cis*-*β*-carotene confirmed the formation of a new peak at 10.5 minutes (see Figure 5) whose mass spectrum matches that expected for 9-*cis*-*β*-apo-10′-carotenal, and whose λ_{max} of 444 nm is consistent with value of 445 nm reported by Alder *et al* [12]. An additional small peak was also detected at 9.8 minutes (λ_{max} 457 nm) in the AtCCD7 reaction. It was found that the peak at 9.8 minutes could be generated from 9-*cis*-*β*-apo-10′-carotenal by heat or UV irradiation, therefore this appears to be an isomeric product. Schwartz et al originally reported that AtCCD7 can cleave all-*trans*-β-carotene [35], but it was later reported that AtCCD7 preferentially cleaves 9-*cis*-β-carotene [12,36]. Hence this peak could be a small amount of the all-*trans* isomer of *β*-apo-10′-carotenal (reported λ_{max} 452 nm), resulting from cleavage of some all-*trans*-*β*-carotene impurity in the reaction, however, Bruno *et al* have reported that CCD7 is selective for the 9-*cis* isomer of *β*-carotene [37]. Surprisingly, no inhibition of CCD7 was observed by any of the hydroxamic acid compounds. We note that the amino acid sequence of CCD7 is divergent from other members of the CCD enzyme family, hence CCD7 may have a somewhat different active site structure that renders it resistant to inhibition.

Biochemical characterisation of AtCCD8. The third enzyme on the strigolactone biosynthesis pathway, CCD8, is responsible for the biosynthesis of the intermediate carlactone [12]. Interestingly, CCD8 catalyses a double oxygenation reaction on the 9-*cis*-*β*-apo-10′-carotenal substrate, forming an enol ether lactone, hence the catalytic mechanism of CCD8 is likely to be different to that of other CCDs. A continuous UV-vis assay was developed for AtCCD8, which was used to study the kinetic and catalytic properties of this enzyme. Pre-steady state kinetic analysis of CCD8 using UV-vis stopped flow experiments gave data matching a two-step kinetic mechanism, with rate constants $k_1 = 0.43\ s^{-1}$, $k_2 = 0.06\ s^{-1}$. These data imply two kinetic steps in the CCD8 catalytic cycle, which may correspond to the two consecutive oxygenation steps, but could potentially correspond to physical steps such as substrate binding.

In order to probe further the catalytic mechanism of AtCCD8, a pH-rate profile was performed, which revealed two inflexions at pH 6.0 and 8.0, implying the presence of a catalytic base of pK_a 6.0, and a catalytic acid of pK_a 8.0. Catalytic activity was completely lost upon treatment with cysteine-specific reagents iodoacetamide and *N*-ethyl maleimide, implying the presence of an active site cysteine residue [32,33]. We suggest a possible catalytic mechanism in Figure 10 that may rationalise these data. The mechanism involves two Criegee rearrangements, known to occur in the catalytic mechanisms of the non-heme iron-dependent catechol dioxygenases [18]. Such rearrangements are known to require acid catalysis [38], which is consistent with the observed pH-rate profile for CCD8, involving an acidic group of pK_a 8.0. In both Criegee rearrangements the more electron-rich substituent would undergo a 1,2-shift onto the electron-deficient hydroperoxide oxygen, and it is known that electron-rich substituents increase the rate of migration in 1,2-rearrangement reactions [39]. The first oxidative cleavage step releases the 8-carbon by-product of the CCD8 reaction (for which a reduced dialcohol derivative was observed by electrospray mass spectrometry), and generates a covalent intermediate.

Figure 10 – Proposed catalytic mechanism for CCD8

The second half of the catalytic cycle involves homolytic cleavage of the carbon-X bond, requiring an active site X group able to form a stable radical species, for which a cysteine residue would be ideally suited. The identification of an active site cysteine residue in CCD8 by cysteine-directed reagents is therefore

consistent with such a mechanism. The final step of the mechanism would involve oxidation of a lactol intermediate and regeneration of the active site nucleophile X and iron (II) centre. An alternative mechanism for CCD8 has been proposed by Alder *et al* [ref 12, Supporting Information], involving two cycloaddition reactions of dioxygen with an isomerised substrate, forming endoperoxide intermediates.

CCD8 was found to be inhibited in a time-dependent fashion by a number of hydroxamic acid inhibitors in the D and F series at 100 μM concentration. Inhibition of AtCCD8 was only observed by a smaller group of compounds at 10 μM concentration. Most effective inhibition was observed by compounds D13H (82%), D15 (71%), D12 (56%) and D9 (54%), which each contain a 2-carbon unit between the aryl group and the hydroxamic acid functional group. We have previously hypothesised that selectivity for hydroxamic acid CCD enzyme inhibitors could be designed by varying the length of spacer between an aromatic ring and a hydroxamic acid metal-chelating group [22]. The observation that most effective inhibition of CCD8 is observed with a C_2 spacer, compared with optimum inhibition of CCD1 by compounds containing a C_1 or no spacer [22], matches this hypothesis, since the initial oxidative cleavage by CCD8 is at the 13,14 position, compared with 9,10 (9′,10′) cleavage by CCD1. Compounds D2-D7 have previously been shown to cause a shoot branching phenotype in *Arabidopsis* at 100 μM concentration (compounds D8-D32 were not tested in the previous study), with compound D6 showing highest activity *in planta* [22]. Of these compounds, inhibition of CCD8 *in vitro* was observed at 10 μM concentration in this study by compounds D6 (53%), D4 (17%) and D5 (9%). Since these compounds show no inhibition of OsD27 or AtCCD7, the inhibition data strongly imply that the shoot branching phenotype caused by these compounds *in planta* is due to inhibition of CCD8, leading to disruption of the strigolactone biosynthetic pathway. Some inhibition of AtCCD8 was also observed with abamine, a tertiary amine known to inhibit NCED [19]. We have previously suggested that abamine, when protonated at neutral pH, may mimic a tertiary carbocation in the NCED catalytic mechanism [4,22]. The proposed catalytic mechanism for CCD8 also contains carbocation intermediates (see Figure 10), which might explain the observed enzyme inhibition.

The potent inhibition of AtCCD8 by compound D15 is noteworthy, since this compound has also been found to inhibit lateral root branching in *A. thaliana* [24]. Since a deficiency of strigolactones resulting from null mutations in the *max3* and *max4* mutants of *Arabidopsis* was reported to cause either formation of

more lateral roots [40] or to have no effect [24], it was concluded that D15 was not acting via a block in strigolactone biosynthesis (24), so D15 may have other targets in addition to CCD8.

As with other plant hormones, strigolactones have diverse biological functions, from regulating plant architecture to stimulating the germination of parasitic plant seeds, to enhancing growth and branching in arbuscular mycorrhizal fungi [41], and more recent work has shown wider roles of strigolactones in regulation of cell division and meristem dormancy [42]. Application of CCD8 inhibitors to diverse plant species and organs, particularly where genetic studies are not feasible, may reveal other biological functions. Inhibitors of strigolactone biosynthesis may also have applications as agrochemical agents affecting shoot branching and plant development, analogous to the use of gibberellin biosynthesis inhibitors to affect plant structure and yield in cotton [43].

EXPERIMENTAL PROCEDURES

Inhibitor Design and Synthesis. Hydroxamic inhibitors and abamine were designed and synthesised as previously published [22-24]. New hydroxamic acids B2, D20, D21, D30, D31 and D32 were prepared using the same synthetic strategy as previously published [22], involving: alkylation of *N*-Boc-*O*-benzylhydroxylamine with an appropriate alkyl halide and NaH; Boc deprotection using trifluoroacetic acid; DCC coupling with an appropriate carboxylic acid; and debenzylation using H_2/Pd. Synthetic procedures and analytical data can be found in the Supporting Information.

Preparation of 9-cis-β-carotene. All-*trans*-*β*-carotene (99%, Sigma) in hexane (1% (w/v), 20 mL) was added to iodine in hexane (1% (w/v), 10 mL) and incubated in the presence of UV light for 30 minutes at room temperature. Isomers were separated by reverse phase HPLC using a ThermoScientific Acclaim C_{30} column (5 μm, 4.6 x 250 mm) maintained at 4° C at a flow rate of 1 mL min^{-1}. Column was eluted with 75:25 methanol:acetonitrile, shifting to 25:35:50 acetonitrile:methanol:tertbutylmethylether over 20 minutes. The gradient was held for a further 5 minutes before returning to 75:25 methanol:acetonitrile for a final five minutes. Retention time of 9-*cis*-*β*-carotene: 24.5 minutes. λ_{MAX}: 448, 474 nm. ε at 475 nm: 6.55 x 10^4 $M^{-1}cm^{-1}$. Retention time of all-*trans*-*β*-carotene: 23.9 minutes. λ_{MAX}: 452, 476 nm.

Gene cloning and expression. OsD27 cDNA was purchased from Genscript and subcloned into the pGEX-4T-1 plasmid. The pGEX-4T-1-OsD27 plasmid was used to transform *E. coli* containing the pBB541 plasmid (Addgene), containing the GroES and GroEL chaperones [44]. The pGEX-4T-1-AtCCD7 plasmid (lacking the first 93 base pairs of AtCCD7, corresponding to a putative chloroplast transit peptide) was used to transform *E. coli* containing the pBB541 plasmid. The pET-151-AtCCD8 plasmid (lacking the first 168 base pairs of AtCCD8, corresponding to a putative chloroplast transit peptide) was used to transform *E. coli* BL21.

E. coli (500 mL) containing the desired plasmids was grown to OD_{600}=0.6 AU and induced with 1 mM IPTG. Cells were harvested at 4220 x g at 4 °C for 20 minutes. Cell pellet was resuspended in PBS buffer (Sigma) pH 7.3 plus 0.05% Triton X-100 (Sigma), 1 mM PMSF (Sigma) and 5 mM DTT (Sigma). Cells were lysed by cell disruption at 20.1 kpsi before centrifugation at 20300 x g at 4 °C for 20 minutes. Cell free extract solution containing over expressed OsD27 was added to a 2 mL GST-Gravitrap column (GE Life Science) for OsD27 and AtCCD7 or a 1 mL HisTrap-Gravitrap column (GE Life Sciences) for AtCCD8 prepared according to the manufacturer's instructions. Cell free extract was passed through the column a total of three times. For GST purification the column was washed with PBS buffer pH 7.3 (25 mL) and eluted with PBS buffer pH 7.3 (10 mL) plus 20 mM reduced glutathione. For N-His_6 purification the column was washed with 50 mM sodium hydrogen phosphate, 300 mM sodium chloride, 20 mM imidazole, pH 8.0 (25 mL) before elution into 50 mM sodium hydrogen phosphate, 300 mM sodium chloride, 250 mM imidazole, pH 8.0 (10 mL). Protein was then concentrated using a 10 kDa centrifugal filter unit before buffer exchange using a PD10 gel filtration column (GE Life Sciences) used according to the manufacturer's instructions. Protein was eluted into 100 mM bis-tris buffer pH 6.7 (3.5 mL) plus 10% glycerol (v/v) and concentrated further in a 10 kDa centrifugal filter. Protein concentration was determined using the Bio-Rad protein assay reagent, using bovine serum albumen as standard.

Biochemical analysis and assays of OsD27. *In vitro* assays were based on methods previously published (12) and were conducted in a final volume of 200 µL. OsD27 enzyme (10 µL, 40 µg) was incubated with 100 mM MOPS, 0.2 (v/v) Triton X-100, 1 mg mL^{-1} catalase, pH 6.4 with 1 µM $FeSO_4$ and 1 µM 2-mercaptoethanol for 10 minutes. 9-*cis*-*β*-carotene in ethanol was added to a final concentration of 20 µM and assays were incubated in the dark for 20 minutes at 25° C with shaking at 180 rpm. Assays were

stopped with the addition of 400 µL 4:1:4 acetone:petroleum ether:diethyl ether and the resulting solution was centrifuged at 4220 x g for five minutes. The organic phase was evaporated under reduced pressure. The residue was resuspended in methanol (200 µL) and analysed by HPLC using the method detailed for the purification of 9-*cis*-*β*-carotene.

For inhibition assays inhibitors were dissolved in either DMSO or ethanol (except silver acetate which was dissolved in water) and a total of 2 µL was added to assays to give a final concentration of 100 µM. Inhibitors were pre-incubated with enzyme for 10 minutes prior to the addition of substrate. Inhibition was calculated from peak areas determined by integration compared to control assays. pH-rate profile experiments were performed as described above, except that the assay buffer was replaced by 100 mM sodium acetate buffer (pH 4.1-5.6), 100 mM PBS buffer (pH 6.7) or 100 mM Tris-HCl (pH 7.7-10.3). For oxygen dependence assays, assays were set up as described above in a two-necked glass apparatus, which was thoroughly degassed and flushed three times with nitrogen gas, prior to incubation of enzyme and substrate under an atmosphere of nitrogen. UV assays were performed in a total volume of 50 µL in an Eppendorf cuvette containing approximately 50 µg of protein in 100 mM bis-tris buffer pH 6.4 plus 10% glycerol (v/v) and 0.1% Triton X-100 (v/v). Hydrogen peroxide, 2-mercaptoethanol, sodium dithionite, sodium dithionite / pyridine, lead acetate and silver acetate were all used at a final concentration of 100 µM.

Protocol for in vivo D27 Assay. pGEX-4T-1-OsD27 was used to transform competent pAC-BETA BL21 *E. coli.* LB media (10 mL) containing appropriate the antibiotic 35 µg mL^{-1} chloramphenicol and 100 µg mL^{-1} ampicillin was inoculated with a single colony of pGEX-4T-1-OsD27 pAC-BETA *E. coli* BL21 and grown overnight at 37º C, 180 rpm. LB media (200 mL) containing appropriate antibiotics was inoculated with the overnight culture and grown at 37º C, 180 rpm until OD at 600 nm = 0.6 AU. IPTG was added to a final concentration of 1 mM. Cultures were incubated overnight at 20º C, 180 rpm, harvested at 4220 x g at 4º C for 15 minutes and then resuspended in water (5 mL). Lysozyme was added to give a final concentration of 25 µg mL^{-1}. Following incubation at room temperature for 10 minutes, cells were lysed by sonication at 50 Hz. *n*-Butanol (1 mL) was added and the organic phase was collected following centrifugation at 4220 x g at 4º C for 10 minutes. The butanol was added to a 100 mg 1 mL Agilnet Bond Elut C_{18} solid phase extraction column and centrifuged at 2000 x g at 4º C for 2 minutes. The column was washed with 10 x 1 mL water before the *β*-carotene was eluted into TBME (1 mL). TBME was removed under reduced pressure and the

residue resuspended into 200 µL methanol. Samples were analysed via HPLC using a ThermoScientific Acclaim C_{30} reversed phase column using the same method described for the purification of 9-*cis*-*β*-carotene.

Assays of AtCCD7. *In vitro* assays of AtCCD7 were performed in a total volume of 200 µL based on previously published methods [12]. AtCCD7 (10 µL, 30µg) was added to 100 mM HEPES, 1 mM TCEP (Sigma), 1 mg mL^{-1} catalase, 0.05% Triton X-100, pH 7.8 with 1 µM $FeSO_4$ and 1 µM sodium ascorbate and incubated at room temperature for 10 minutes. 9-*cis*-*β*-carotene was added to a final concentration of 20 µM and assays were incubated at 25° C in the dark for 20 minutes with shaking at 180 rpm. Assays were stopped with the addition of 200 µL 4 M NaCl and 200 µL ethyl acetate. The resulting solution was centrifuged at 4220 x g for five minutes and the organic phase was desalted with 100 mg 1 mL C_{18} solid phase extraction cartridges (Agilent Bond Elut), washing with 10 x 1 mL water and eluting into 400 µL tertbutylmethylether. Organic solvent was removed under reduced pressure and resuspended in methanol. Analysis was performed via HPLC using the method described above for the purification of 9-*cis*-*β*-carotene (retention time 10.5 min; λ_{max} 444 nm; HRMS 377.2839, calc. 377.2840 for $C_{27}H_{37}O^+$ (MH^+)). Inhibition assays were performed at 100 µM inhibitor concentration, as described for OsD27.

Biochemical analysis and assays of AtCCD8. The substrate 9-*cis*-*β*-apo-10′-carotenal was prepared from assays of AtCCD7 with 9-*cis*-*β*-carotene as described above. Collected 9-*cis*-*β*-apo-10′-carotenal was concentrated under reduced pressure and resuspended in ethanol. *In vitro* assays were performed in a total volume of 200 µL using a 96 well microtitre plate reader, recording at 430 nm. AtCCD8 (10 µL, 40 µg) was added to 100 mM HEPES, 1 mM TCEP, pH 7.8 containing 10 µM 9-*cis*-*β*-apo-10′-carotenal, 1 µM $FeSO_4$ and 1 µM sodium ascorbate. Inhibition assays were performed at 100 µM and 10 µM inhibitor concentration, as described for OsD27.

Stopped flow experiments were performed at the University of Manchester Institute of Biotechnology using an Applied Photophysics SX.18MV stopped flow spectrometer with a 05169 pbp monochromator. 9-*cis*-*β*-apo-10'-carotenal substrate was prepared as described, with the exception that prior to the removal of 4:1:4 acetone : petroleum ether : diethyl ether under vacuum, 0.04% (v/v) Triton X-100 was added and the residue was resuspended into water. Reactions were performed in a 1:1 molar ratio of 9-

cis-*β*-apo-10′-carotenal:AtCCD8 at a concentration of 12 μM substrate and 12 μM AtCCD8 in 100 mM HEPES buffer pH 7.8 containing 1 mM TCEP. For determination of the kinetic parameters k_1 and k_2, analysis was performed using Applied Photophysics Pro-Data SX software and the enzyme was diluted relative to the substrate.

pH rate profile experiments were performed as described for OsD27. Assays with group specific reagents were performed by preincubation of AtCCD8 with group specific reagents at a final concentration of 1 mM for 10 minutes before addition of substrate, then monitoring at 430 nm as described above.

REFERENCES

1. Walter MH and Strack D (2011) Carotenoids and their cleavage products: Biosynthesis and functions. *Nat. Prod. Rep.*, **28**, 663-692.
2. Harrison PJ and Bugg TDH (2014) Enzymology of the carotenoid cleavage dioxygenases: Reaction mechanisms, inhibition and biochemical roles. *Arch. Biochem. Biophys.* **544**, 105-111.
3. Schwartz SH, Tan BC, Gage DA, Zeevaart JAD and McCarty DR (1997) Specific oxidative cleavage of carotenoids by VP14 of maize. *Science*, **276**, 1872-1874.
4. Taylor IB, Sonneveld T, Bugg TDH and Thompson AJ (2005) Regulation and manipulation of the biosynthesis of abscisic acid, including the supply of xanthophyll precursors. *J. Plant Growth Regul.* **24**, 253-273.
5. Iuchi S, Kobayashi M, Taji T, Naramoto M, Seki M, Kato T, Tabata S, Kakubari Y, Yamaguchi-Shinozaki K and Shinozaki K (2001) Regulation of drought tolerance by gene manipulation of 9-*cis*-epoxycarotenoid dioxygenase, a key enzyme in abscisic acid biosynthesis in *Arabidopsis*. *Plant J.* **27**, 325-333.
6. Nambara E and Marion-Poll A (2005) Abscisic acid biosynthesis and catabolism. *Annu. Rev. Plant Biol.* **56**, 165-185.
7. Yan W, Jang G-F, Haeseleer F, Esumi N, Chang J, Kerrigan M, Campochiaro M, Campochiaro P, Palczewski K and Zack DJ (2001) Cloning and characterization of a human β,β-carotene-15, 15′-dioxygenase that is highly expressed in the retinal pigment epithelium. *Genomics*. **72**, 193-202.

8. Redmond TM, Gentleman S, Duncan T, Yu S, Wiggert B, Gnatt E and Cunningham FX (2001) Identification, expression, and substrate specificity of a mammalian β-carotene 15,15′-dioxygenase. *J. Biol. Chem*. **276**, 6560-6565.
9. Akiyama K, Matsuazaki K-I and Hayashi H (2005) Plant sesquiterpenes induce hyphal branching in arbuscular mycorrhizal fungi. *Nature* **435**, 824-827.
10. Gomez-Roldan V, Fermas S, Brewer PB, Puech-Pages V, Dun EA, Pillot J-P, Letisse F, Matusova R, Danoun S, Portais S-C, Bouwmeester H, Becard G, Beveridge CA, Rameau C, and Rochange SF (2008) Strigolactone inhibition of shoot branching. *Nature* **455**, 189.
11. Umehara M, Hanada A, Yoshidam S, Akiyama K, Arite T, Takeda-Kamiya N, Magome H, Kamiya Y, Shirasu K, Yoneyama K, Kyozuka J and Yamaguchi S (2008) Inhibition of shoot branching by new terpenoids plant hormones. *Nature* **455**, 195-200.
12. Alder A, Jamil M, Marzorati M, Bruno M, Vermathen M, Bigler P, Ghisla S, Bouwmeester H, Beyer P and Al-Babili S (2012) The path from β-carotene to carlactone, a strigolactone-like plant hormone. *Science*, 335, 1348-1351.
13. Lin H, Wang R, Qian Q, Yan M, Meng X, Fun Z, Yan C, Jiang B, Su Z, Li J and Wang J (2009) DWARF27, an iron-containing protein required for the biosynthesis of strigolactones, regulates rice tiller bud outgrowth. *Plant Cell* **21**, 1512-1525.
14. Abe S, Sado A, Tanaka K, Kisugi T, Asami K, Ota S, Kim HI, Yoneyama K, Xie X, Ohnishi T, Seto Y, Yamaguchi S, Akiyama K, Yoneyama K and Nomura T (2014) Carlactone is converted to carlactonoic acid by MAX1 in *Arabidopsis* and its methyl ester can directly interact with AtD14 *in vitro*. *Proc. Natl. Acad. Sci. USA.* **111**, 18084-18089.
15. Zhang Y, van Dijk AD, Scaffidi A, Flematti GR, Hofmann M, Charnikhova T, Verstappen F, Hepworth J, van der Krol S, Leyser O, Smith SM, Zwanenburg B, Al-Babili S, Ruyter-Spira C and Bouwmeester HJ (2014) Rice cytochrome P450 MAX1 homologs catalyze distinct steps in strigolactone biosynthesis. *Nat. Chem. Biol*. **10**, 1028-1033.
16. Kloer DP, Ruch S, Al-Babili S, Beyer P and Schulz GE (2005) The structure of a retinal-forming carotenoid oxygenase. *Science* **308**, 267-269.

17. Messing S, Gabelli S, Echeverria I, Vogel JT, Guan J-C, Tan B-C, Klee HJ, McCarty CR and Amzel L-M (2010) Structural insights into maize Viviparous14, a key enzyme in the biosynthesis of the phytohormone abscisic acid. *Plant Cell*, **22**, 2970-2980.

18. Bugg TDH (2003) Dioxygenase enzymes: catalytic mechanisms and chemical models. *Tetrahedron*, **59**, 7075-7101.

19. Han SY, Kitahata N, Sekimata K, Saito T, Kobayashi M, Nakashima K, Yamaguchi-Shinozaki K, Yoshida S and Asami T (2004) A novel inhibitor of 9-*cis*-epoxycarotenoid dioxygenase in abscisic acid biosynthesis in higher plants. *Plant Physiol*. **135**, 1574-1582.

20. Kitahata N, Han S-Y, Noji N, Saito T, Kobayashi M, Nakano T, Kuchitsu K, Shinozaki K, Yoshida S, Matsumoto S, Tsujimoto M and Asami T (2006). A 9-*cis*-epoxycarotenoid dioxygenase inhibitor for use in the elucidation of abscisic acid action mechanisms. *Bioorg. Med. Chem*. **14**, 5555-5561.

21. Boyd J, Gai Y, Nelson KM, Lukiwski E, Talbot J, Loewen MK, Owen S, Zaharia LI, Cutler AJ, Abrams SR and Loewen MC (2009) Sesquiterpene-like inhibitors of a 9-*cis*-epoxycarotenoid dioxygenase regulating abscisic acid biosynthesis in higher plants. *Bioorg. Med. Chem.*, **17**, 2902-2912.

22. Sergeant MJ, Li JJ, Fox C, Brookbank N, Rea D, Bugg TDH, and Thompson AJ (2009) Selective inhibition of carotenoid cleavage dioxygenases: phenotypic effects on shoot branching. *J. Biol. Chem.* **284**, 5257-5264.

23. Sergeant MJ, Harrison PJ, Jenkins R, Moran G, Bugg TDH and Thompson AJ (2013) Phytotoxic effects of selected *N*-benzyl-benzoylhydroxamic acid metallo-oxygenase inhibitors: investigation into mechanism of action. *New J. Chem*. **37**, 3461-3465.

24. Van Norman J, Zhang J, Cazzonelli C, Pogson B, Harrison PJ, Bugg TDH, Chan K-X, Thompson AJ & Benfrey PN (2014) Periodic root branching in *Arabidopsis* requires synthesis of an uncharacterized carotenoid derivative. *Proc. Natl. Acad. Sci. USA*. **111**, E1300-E1309.

25. Sainsbury PD, Mineyeva Y, Mycroft Z and Bugg TDH (2015) submitted for publication.

26. Tsukida K, Saiki K, Takii T and Koyama Y (1982) Separation and determination of *cis*/*trans*-β-carotenes by high-performance liquid chromatography. *J. Chromatogr. A*, 3, 359-364.

27. Emenhiser C, Sander LC and Schwartz SJ (1995) Capability of a polymeric C_{30} stationary phase to resolve *cis-trans* carotenoid isomers in reversed-phase liquid chromatography. *J. Chromatogr. A*, 707, 205-216.

28. Cunningham FX, Pogson B, Sun ZR, McDonald KA, DellaPenna D, and Gantt E (1996) Functional analysis of the beta and epsilon lycopene cyclase enzymes of *Arabidopsis* reveals a mechanism for control of cyclic carotenoid formation. *Plant Cell*, 8, 1613-1626.

29. Fee JA, Findling KL, Yoshida T, Hille R, Tarr GE, Hearshen DO, Dunham WR, Day EP, Kent TA and Münck E (1983) Purification and characterization of the Rieske iron-sulfur protein from *Thermus thermophilus*. Evidence for a [2Fe-2S] cluster having non-cysteine ligands. *J. Biol. Chem.*, **259**, 124-133.

30. Tagawa K and Arnon DI (1968) Oxidation-reduction potentials and stoichiometry of electron transfer in ferredoxins. *Biochem. Biophys. Acta*, **153**, 602-613.

31. Xu FF and Imlay JA (2012) Silver (I), mercury (II), cadmium (II), and zinc (II) target exposed enzymic iron-sulfur clusters when they toxify *Escherichia coli*. *Appl. Environ. Microbiol.* **78**, 3614-3621.

32. Reymond J-L, Jahangiri GK, Stoudt C, and Lerner RA (1993) Antibody catalysed hydrolysis of enol ethers. *J. Am. Chem. Soc*. **115**, 3909-3917.

33. Gadda G, Banerjee A, Dangott LJ, and Fitzpatrick PF (2000) Identification of a cysteine residue in the active site of nitroalkane oxidase by modification with *N*-ethylmaleimide. *J. Biol. Chem*. **275**, 31891-31895.

34. Fox BS and Walsh CT (1983) Mercuric reductase: homology to glutathione reductase and lipoamide dehydrogenase. Iodoacetamide alkylation and sequence of the active site peptide. *Biochemistry* **22**, 4082-4088.

35. Schwartz SH, Qin XQ, and Loewen MC (2004) The biochemical characterization of two carotenoid cleavage enzymes from *Arabidopsis* indicates that a carotenoid-derived compound inhibits lateral branching. *J. Biol. Chem.*, **279**, 46940-46945.

36. Alder A, Holderman I, Beyer P and Al-Babili S (2008) Carotenoid oxygenases involved in plant branching catalyse a highly specific conserved apocarotenoid cleavage reaction. *Biochem. J.*, **416**, 289-296.

37. Bruno M, Hofmann M, Vermathen M, Alder A, Beyer P, and Al-Babili S (2014) On the substrate- and stereospecificity of the plant carotenoid cleavage dioxygenase 7. *FEBS Lett*. **588**, 1802-7.
38. Mendel S, Arndt A and Bugg TDH (2004) Acid-base catalysis in the extradiol catechol dioxygenase reaction mechanism: site-directed mutagenesis of His-115 and His-179 in *Escherichia coli* 2,3-dihydroxyphenylpropionate 1,2-dioxygenase (MhpB). *Biochemistry*, **43**, 13390-13396.
39. Lowry TH, Richardson KS "Mechanism and theory in organic chemistry" 3rd edition, 1987, p. 501-504, Harper Collins, New York.
40. Koltai H (2011) Strigolactones are regulators of root development. *New Phytologist*, **190**, 545-549.
41. Xie X, Yoneyama K, and Yoneyama K (2010) The strigolactone story. *Annu. Rev. Phytopathol*., **48**, 93-117.
42. Mason MG (2013) Emerging trends in strigolactone research. *New Phytologist*, **198**, 975-977.
43. Ren X, Zhang L, Du M, Evers JB, van der Werf W, Tian X, and Li Z (2013) Managing mepiquat chloride and plant density for optimal yield and quality of cotton. *Field Crops Res*., **149**, 1-10.
44. de Marco A (2007) Protocol for preparing proteins with improved solubility by co-expressing with molecular chaperones in *Escherichia coli. Nat. Protocols*, **2**, 2632-2639.

Acknowledgements. We thank Joshua Cartwright, Samuel Lowe and Mohsina Kahn (University of Warwick) for additional synthetic work. We thank Dr. David Brocklehurst (Syngenta, Jealott's Hill, Bracknell, UK) for helpful advice and practical assistance, and Dr. Jaimie van Norman and Dr. Philip Benfey (Duke University) for helpful discussions.

FOOTNOTES

*This work was supported by a BBSRC / Syngenta CASE funded PhD studentship to PJH.

FIGURE LEGENDS

FIGURE 1. The strigolactone biosynthesis pathway from all-*trans*-*β*-carotene to *ent*-2'-*epi*-5-deoxystrigol.

FIGURE 2. HPLC analysis of the reaction catalysed by OsD27. A: all-*trans*-*β*-carotene extracted from pAC-BETA *E. coli* (empty vector control). B: *β*-carotene extracted from pAC-BETA pGEX-OsD27 *E. coli* incubation (*in vivo* transformation by D27). C: authentic all-*trans*-*β*-carotene (95%, Sigma) control. D: reaction of all-*trans*-*β*-carotene with recombinant OsD27 in 100 mM MOPS buffer pH 6.4. E: purified 9-*cis*-*β*-carotene. F: reaction of 9-*cis*-*β*-carotene with recombinant OsD27 in 100 mM MOPS buffer pH 6.4. Peak assignments: 1 – all-*trans*-*β*-carotene; 2 – 9-*cis*-*β*-carotene; 3 – isomer of *β*-carotene.

FIGURE 3. UV-Vis spectrum of OsD27 (blue line), showing absorbance peak at λ_{max} 422 nm; and spectrum of OsD27 following incubation with silver acetate (red line).

FIGURE 4. A. pH rate profile for the OsD27 catalysed isomerisation of 9-*cis*-*β*-carotene to all-*trans*-*β*-carotene B. Effect of additives on the ratio of all-trans-*β*-carotene : 9-*cis*-*β*-carotene following the reaction of 9-*cis*-*β*-carotene with recombinant OsD27. Reactions are shown with the respective control for each experiment (black bars).

FIGURE 5. HPLC analysis of the CCD7-catalysed reaction of 9-*cis*-*β*-carotene. A: 9-*cis*-*β*-carotene. B: 9-*cis*-*β*-carotene plus CCD7. Peak assignments: **1**, 9-*cis*-*β*-carotene; **2**, all-*trans*-*β*-carotene; **3**, 9-*cis*-*β*-apo-10′-carotenal.

FIGURE 6. Monitoring of CCD8-catalysed cleavage of 9-*cis*-*β*-apo-10′-carotenal by UV-vis spectroscopy and mass spectrometry. A: decrease in absorbance at 430 nm observed for 1- and 2-fold concentrations of CCD8. B: Absorbance change observed for boiled enzyme control. C: derivatives of carlactone and C_8 product detected by electrospray mass spectrometry.

FIGURE 7. A: UV-visible scanning of the CCD8-catalysed reaction of 9-*cis*-*β*-apo-10′-carotenal at 0.01-200 sec. B: Decrease in absorbance at 440 nm (dashed line) observed from stopped flow analysis of the CCD8 cleavage reaction at 0.01-40 sec; with observed fit to second order exponential (dotted line).

FIGURE 8. A: pH rate profile of CCD8 cleavage reaction of 9-*cis*-*β*-apo-10′-carotenal. B: Percentage activity of CCD8 cleavage reaction in the presence of different additives, relative to control cleavage reaction.

FIGURE 9. Proposed catalytic mechanism for carotenoid *cis*-*trans* isomerisation catalysed by OsD27.

FIGURE 10. Proposed catalytic mechanism for CCD8, involving an active site nucleophile X, probably a cysteine residue, and an acidic residue A of pK_a 8.0.

TABLE 1. Inhibition data for OsD27 at 100 µM and for AtCCD8 at 100 µM and 10 µM. Chemical structures of hydroxamic acids shown below.

Inhibitor				D27	CCD8	
Class	Name	X	Y	Inhibition at 100 µM (%)	Inhibition at 100 µM (%)	Inhibition at 10 µM (%)
Aryl-CON(OH)-Aryl	F1	4-OMe	H	10	>95	<5
	F2	4-OMe	F	16	>95	<5
	F3	3,4-$(OMe)_2$	H	9	>95	<5
	F4	3,4-$(OMe)_2$	F	25	>95	<5
	F5	3-Cl	H	21	>95	<5
	F6	3-NH_2	H	7	>95	21
Aryl-C_1-CON(OH)-Aryl	D1	4-OH	H	0	>95	<5
	D2	4-OH	F	0	>95	<5
	D4	4-OMe	F	0	>95	17
	D5	3,4-$(OMe)_2$	H	0	>95	9
	D6	3,4-$(OMe)_2$	F	0	>95	53
	D7	3,4-OCH_2O-	F	0	>95	25
Aryl-C_1-CON(OH)-Alkyl	D30	4-OMe	$C_{10}H_{17}$	41	70	-
	D20	4-OMe	$(CH_2)_2CO_2Na$	26	47	-
	D21	Naphthyl	$(CH_2)_2CO_2Na$	33	92	-
Aryl-C_2-CON(OH)-Y	D9	4-OMe	CH_2Ph	0	>95	54
	D15	4-OMe	CH_2PhF	0	>95	71
	D10	3,4-$(OMe)_2$	C_8H_{17}	0	>95	<5
	D11	4-OMe	C_8H_{17}	0	>95	<5
	D12	3,4-$(OMe)_2$	H	0	>95	56
	D12H	3,4-$(OMe)_2$	H	40	78	-
	D13	4-OMe	H	0	>95	47
	D13H	4-OMe	H	0	>95	82
Ring-C_5-CON(OH)-Aryl	B1	cyclohexyl	H	0	94	<5
	B2	4-MeOPh	CH_2PhF	40	0	-
Alkyl-CON(OH)-Y	D31	C_9H_{15}	CH_2Ph	38	52	-
	D32	$C_{11}H_{17}$	CH_2Ph	33	47	-
	Abamine	---	---	0	>95	<5

aryl-CON

F1-6

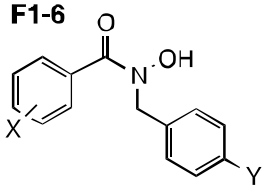

arylC$_1$-CON

D1-7

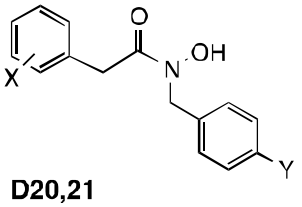

D20,21

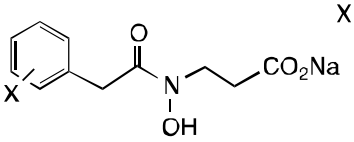

D30

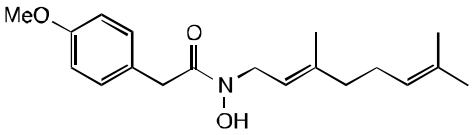

arylC$_2$-CON

D9-11,12H,13H,15

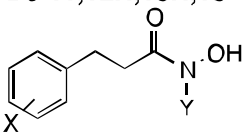

D12,13

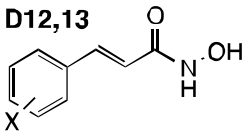

longer acyl

B1

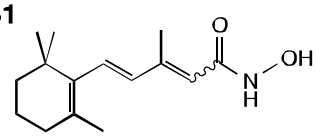

B2

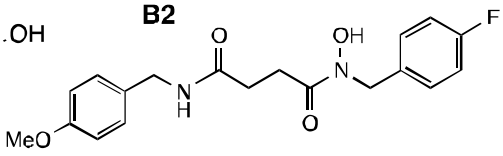

D31

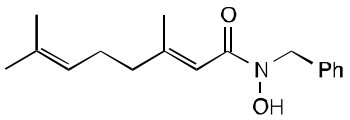

D32

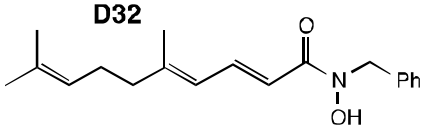

FIGURE 1.

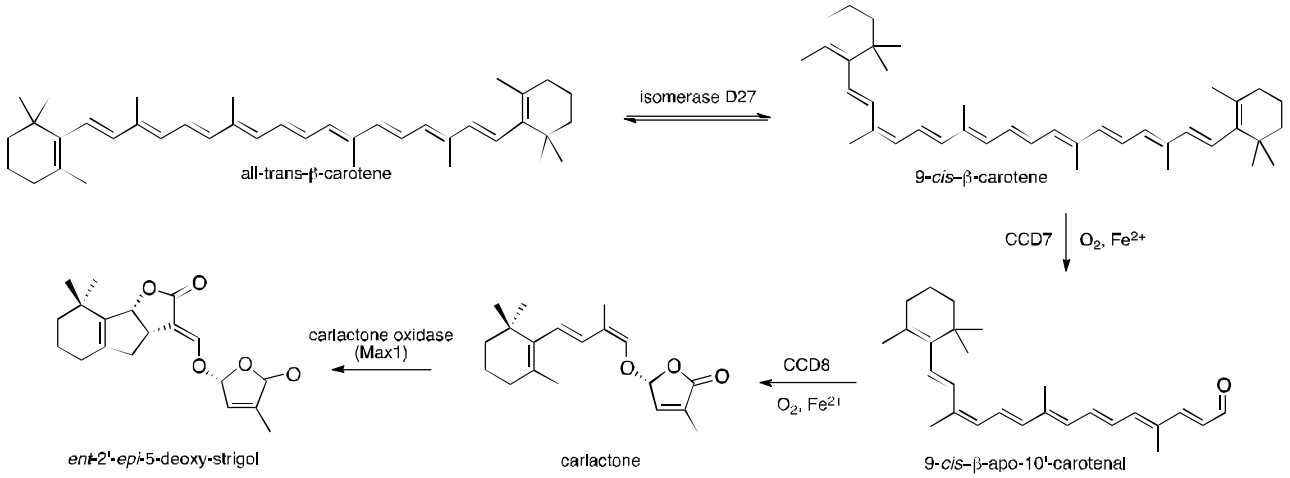
all-trans-β-carotene
isomerase D27
9-cis-β-carotene
CCD7
O2, Fe2+
9-cis-β-apo-10'-carotenal
CCD8
O2, Fe2+
carlactone
carlactone oxidase
(Max1)
ent-2'-epi-5-deoxy-strigol

FIGURE 2.

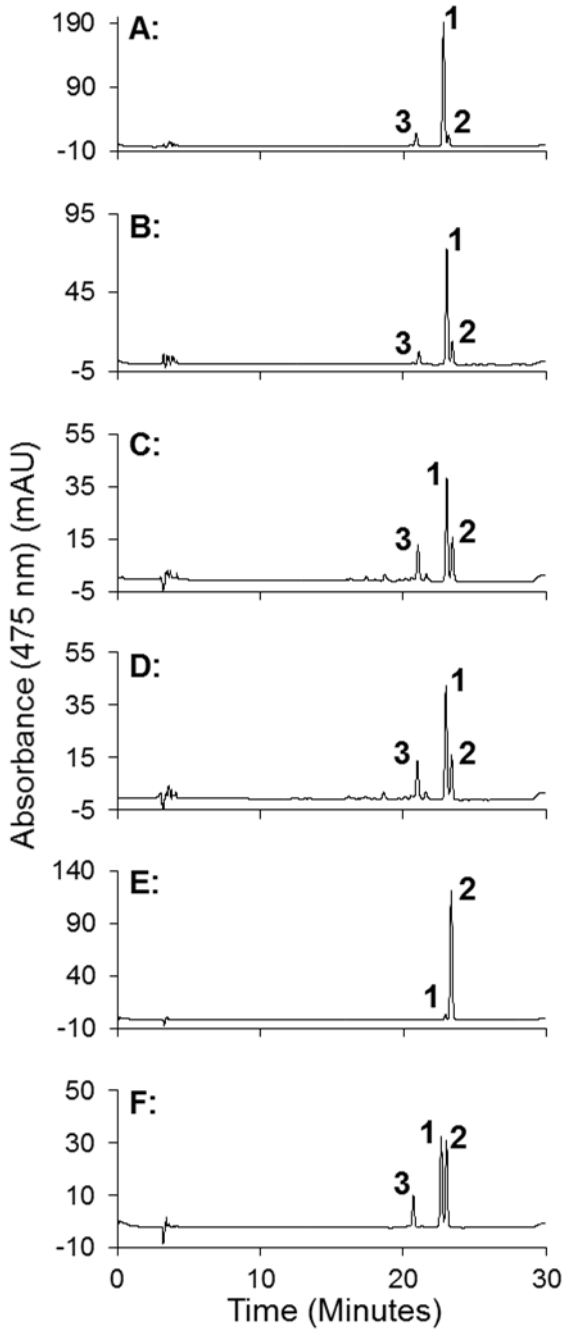
A:
B:
C:
D:
E:
F:
1
2
3
190
90
-10
95
45
-5
55
35
15
-5
55
35
15
-5
140
90
40
-10
50
30
10
-10
0
10
20
30
Time (Minutes)
Absorbance (475 nm) (mAU)

FIGURE 3.

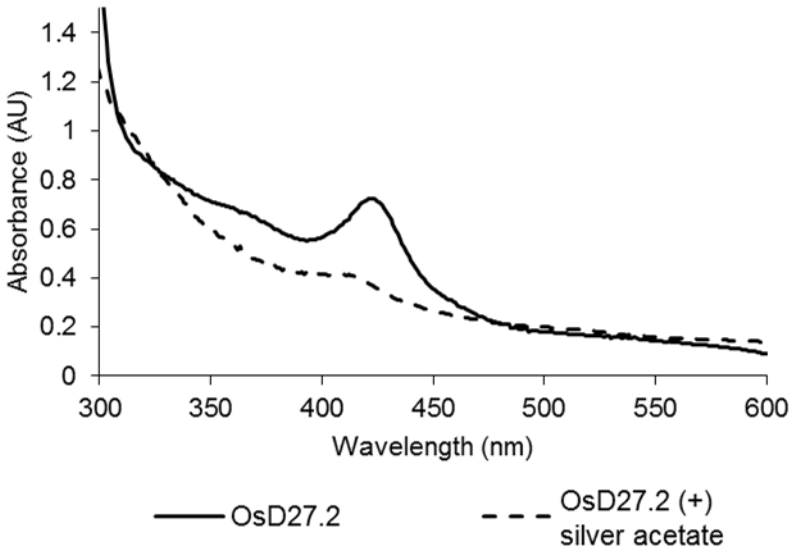

FIGURE 4.

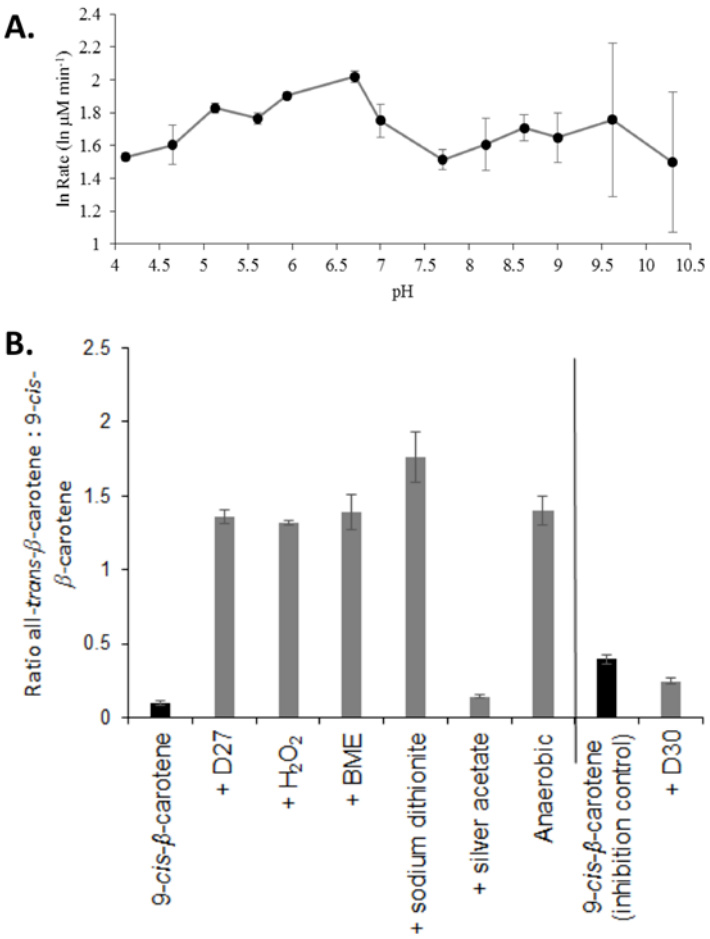

FIGURE 5.

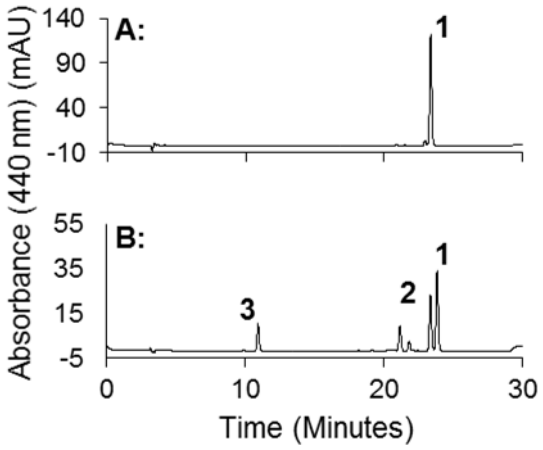
A:
B:
1
2
3
140
90
40
-10
55
35
15
-5
0
10
20
30
Absorbance (440 nm) (mAU)
Time (Minutes)

FIGURE 6.

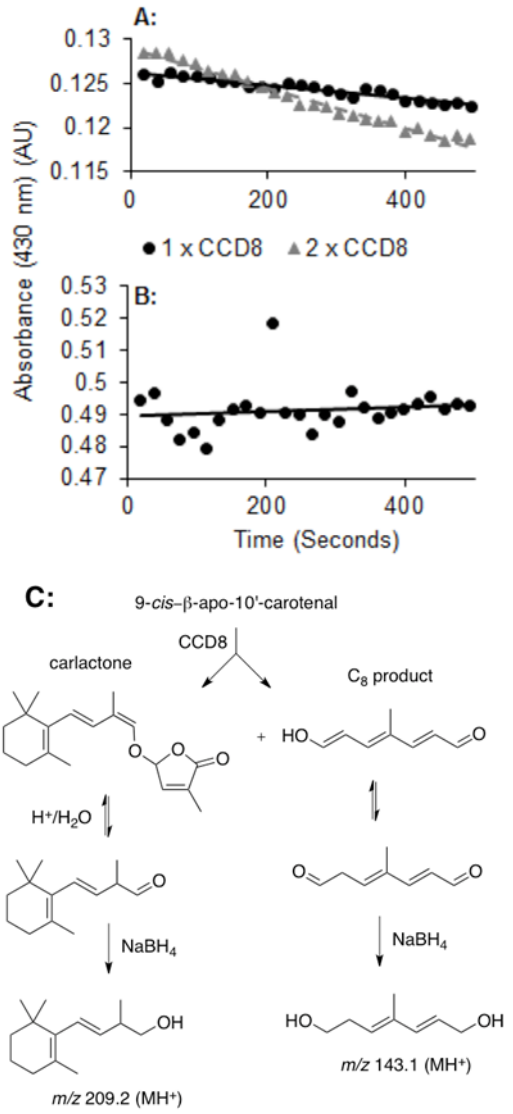
A:
0.13
0.125
0.12
0.115
0
200
400
1 x CCD8
2 x CCD8
B:
0.53
0.52
0.51
0.5
0.49
0.48
0.47
Absorbance (430 nm) (AU)
Time (Seconds)
C:
9-cis-β-apo-10'-carotenal
CCD8
carlactone
C8 product
HO
O
H+/H2O
NaBH4
OH
m/z 209.2 (MH+)
m/z 143.1 (MH+)

FIGURE 7.

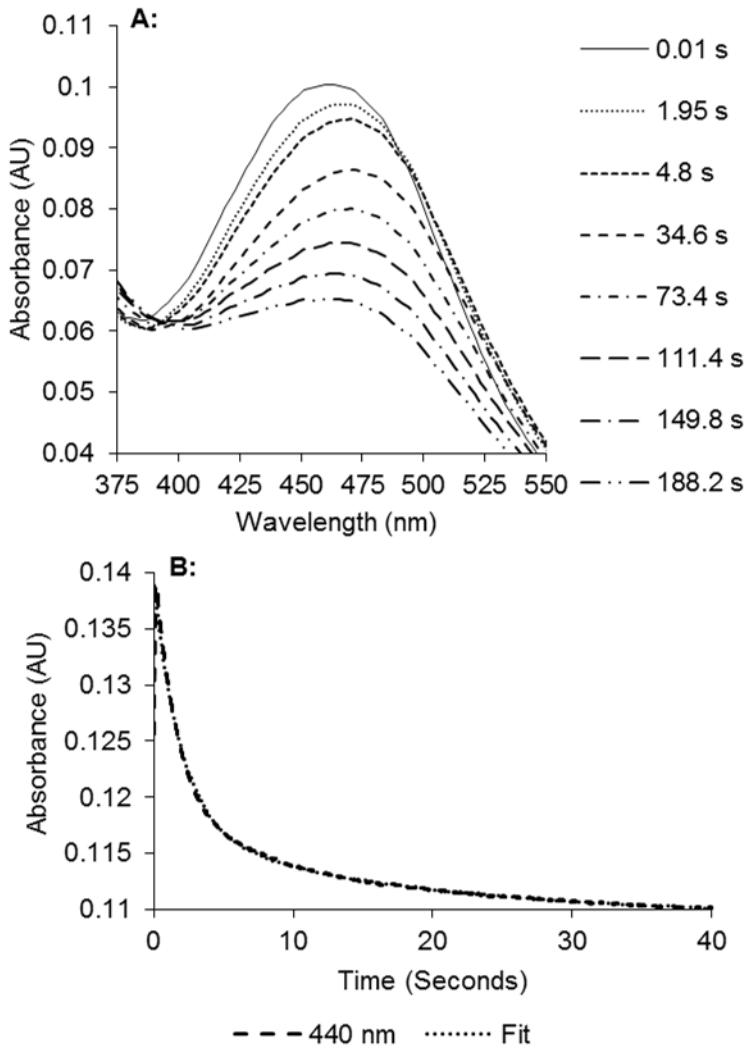
A:
Absorbance (AU)
0.11
0.1
0.09
0.08
0.07
0.06
0.05
0.04
375 400 425 450 475 500 525 550
Wavelength (nm)
0.01 s
1.95 s
4.8 s
34.6 s
73.4 s
111.4 s
149.8 s
188.2 s
B:
Absorbance (AU)
0.14
0.135
0.13
0.125
0.12
0.115
0.11
0 10 20 30 40
Time (Seconds)
440 nm
Fit

FIGURE 8.

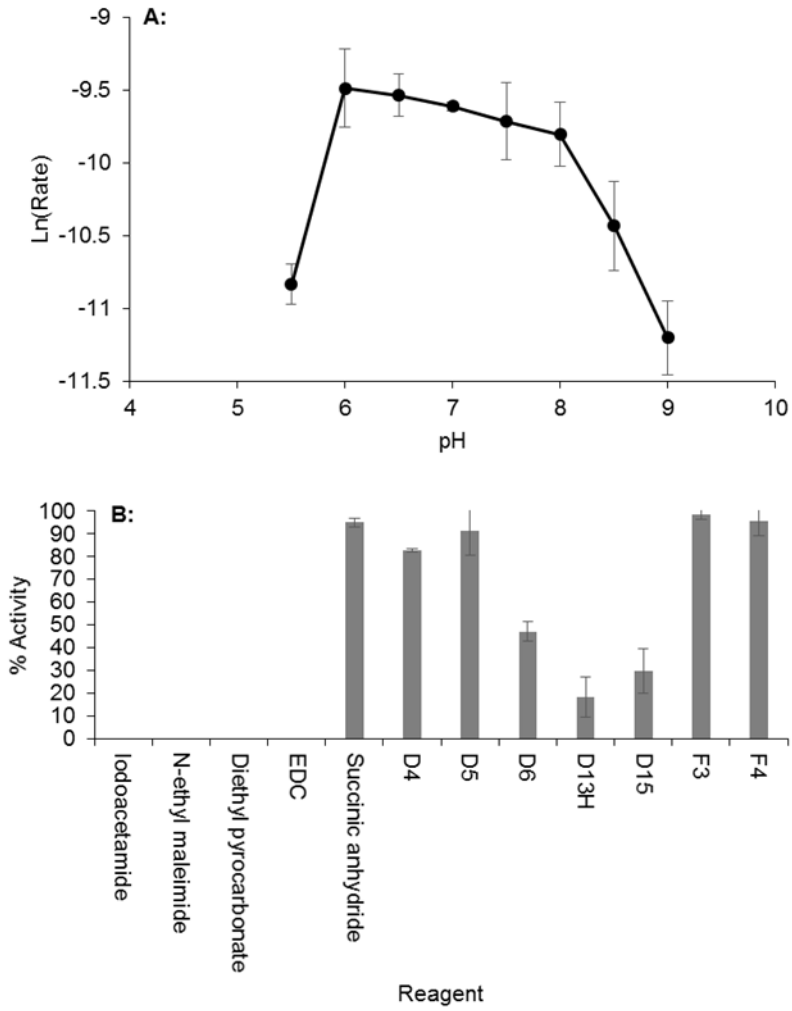
A:
Ln(Rate)
pH
B:
% Activity
Reagent
Iodoacetamide
N-ethyl maleimide
Diethyl pyrocarbonate
EDC
Succinic anhydride
D4
D5
D6
D13H
D15
F3
F4

FIGURE 9

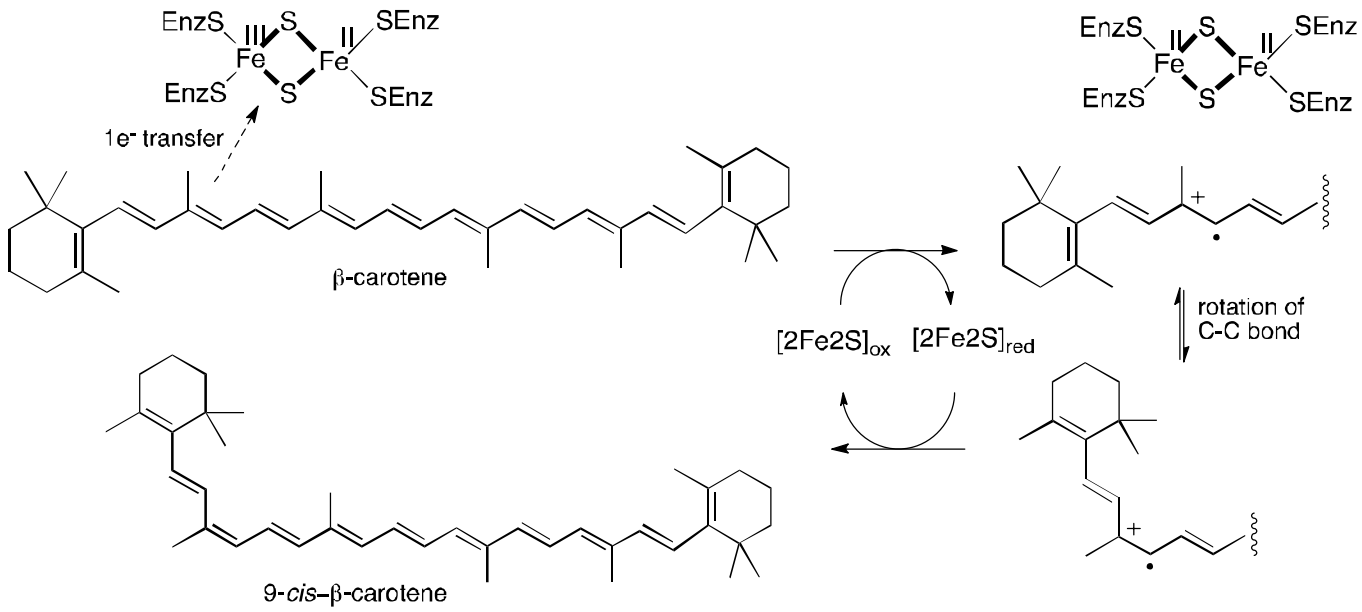
EnzS
S
SEnz
Fe
Fe
EnzS
S
SEnz
1e⁻ transfer
β-carotene
[2Fe2S]ox
[2Fe2S]red
rotation of
C-C bond
9-cis–β-carotene

FIGURE 10

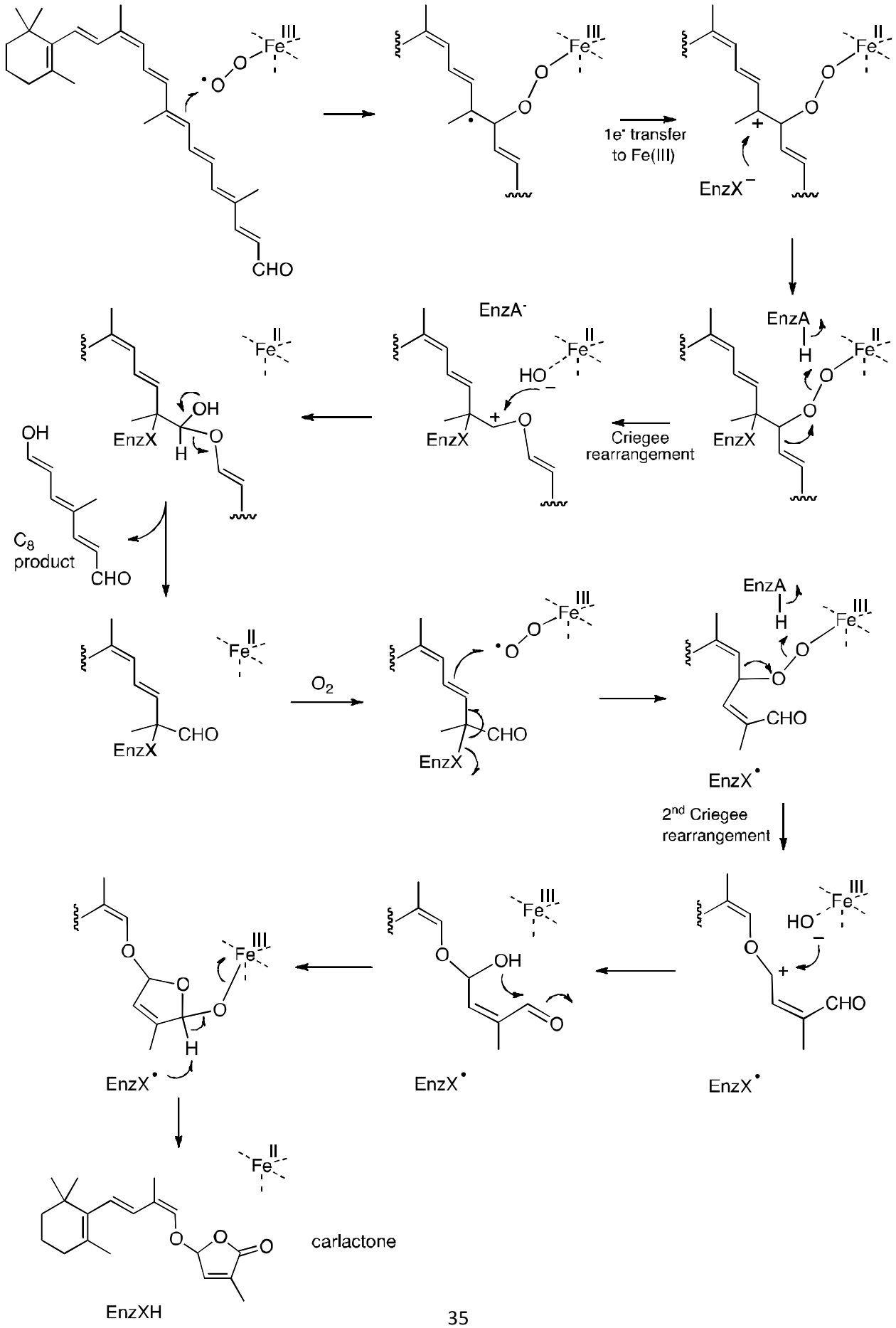
1e⁻ transfer
to Fe(III)
EnzX⁻
EnzA⁻
EnzA
Criegee
rearrangement
C8
product
CHO
OH
EnzX
O2
2nd Criegee
rearrangement
carlactone
EnzXH